

The efforts taken by the authors to address the reviewers' concerns have resulted in a further strengthened paper that would be of broad enough interest to researchers working on isotope ecology/hydrology, and therefore merits publication in HESS.

Response: Thanks for the reviewer for the positive feedbacks.

I have only some minor points to raise, as below:

Lines 112-121: For this section, it seems to me there is still a lack of clarification why the method is called the intersection point method. It can be understood from your description that δ_a and C_a remain constant across two consecutive measurement periods, but there is no further explanation how this local constant concept is related to the intersection point of two Keeling plots. To facilitate understanding by the reader, I would suggest that the authors state more explicitly that the local constant condition would cause two adjacent Keeling plots to intersect at a point that corresponds to the background air (δ_a , $1/C_a$) (and that's where the method name intersection point comes from).

Response: We are grateful for the constructive comments from the reviewer. We agree that further explanation on the origin of intersection point method will improve clarity. We added related content as the reviewer suggested. The detailed addition is as following on line 119:

“Algebraically, δ_a and C_a are common solutions in Eq. (4) and Eq. (5). Geometrically, point $(\delta_a, 1/C_a)$ is the intersection of two Keeling plots at t_1 and t_2 . That is the reason the method was named IP method.”

Line 182: Here it was mentioned that calibration was done to correct for concentration dependence. I'm just wondering if there was any effort made to check/correct drift-induced measurement biases, as instrumental drift may sometimes (although not always) be a non-trivial issue for long-term isotope monitoring in the field.

Response: We are grateful for the constructive comments about a calibration issue from the reviewer. As we need continuous data, the observation should last uninterrupted as long as possible. As a result, the calibration was made in every 5-10 days, which is consistent with the frequency of calibration by other researchers such as Steen-Larsen et al. (2013) who conducted their work in Greenland. According to our calibration data on standards, the average drift (absolute value) was 0.16‰ between two adjacent calibrations. As the precision of the analyzer is 0.04‰ to 0.25‰ for $\delta^{18}\text{O}$, the biases of 0.16‰ should not affect the calculation results. We added the frequency of calibration at the end of this section.

Steen-Larsen, H. C., Johnsen, S. J., Masson-Delmotte, V., Stenni, B., Risi, C., Sodemann, H., Balslev-Clausen, D., Blunier, T., Dahl-Jensen, D., and Ellehøj, M. D.: Continuous monitoring of summer surface water vapor isotopic composition above the Greenland Ice Sheet, **Atmospheric Chemistry and Physics**, 13, 4815-4828, doi:10.5194/acp-13-4815-2013, 2013.

Line 319: negative slope is due to $\delta\text{ET} < \delta a$ and positive slope is due to $\delta\text{ET} > \delta a$
Shouldn't be it the other way around instead, i.e., negative slope is due to $\delta\text{ET} > \delta a$?

Response: We thank the reviewer for pointing this out and we apologize for the oversight. Changed as suggested.

1 **Novel Keeling plot based methods to estimate the isotopic composition of ambient water**
2 **vapor**

3 Yusen Yuan^{a,b}, Taisheng Du^{a*}, Honglang Wang^c, Lixin Wang^{b*}

4
5 ^a Center for Agricultural Water Research in China, China Agricultural University,
6 Beijing 100083, China

7 ^b Department of Earth Sciences, Indiana University-Purdue University Indianapolis,
8 Indianapolis, Indiana 46202, USA

9 ^c Department of Mathematical Sciences, Indiana University-Purdue University
10 Indianapolis, Indianapolis, Indiana 46202, USA

11
12 * Corresponding author: Dr. Taisheng Du
13 Fax: +86-10-62737611; Tel: +86-10-62738398
14 Email: dutaisheng@cau.edu.cn

15
16 * Corresponding author: Dr. Lixin Wang
17 Fax: +1-1-317-274-7966; Tel: +1-317-274-7764
18 Email: lxwang@iupui.edu

19
20
21 **Highlights:**

- 22 1. Two new methods were developed to estimate the isotopic composition of ambient
- 23 vapor.
- 24 2. Theoretical derivations were provided for these two methods.
- 25 3. Linear regression showed strong agreement between the two methods.
- 26 4. The methods provide a possibility to calculate the proportion of evapotranspiration
- 27 fluxes to total atmospheric vapor using the same instrumental setup for the traditional
- 28 Keeling plot investigations.

30 **Abstract**

31 Keeling plot approach, a general method to identify the isotopic composition of source
32 atmospheric CO₂ and water vapor (i.e., evapotranspiration), has been widely used in terrestrial
33 ecosystems. The isotopic composition of ambient water vapor (δ_a), an important source of
34 atmospheric water vapor, is not able to be estimated to date using the Keeling plot approach.
35 Here we proposed two new methods to estimate δ_a using the Keeling plots: one using
36 intersection point method and another relying on the Intermediate Value Theorem. As actual δ_a
37 value was difficult to measure directly, we used two indirect approaches to validate our new
38 methods. First, we made external vapor trackings using Hybrid Single Particle Lagrangian
39 Integrated Trajectory (HYSPLIT) model to facilitate explaining the variations of δ_a . The
40 trajectory vapor origin results were consistent with the expectations of the δ_a values estimated
41 by these two methods. Second, regression analysis was used to evaluate the relationship
42 between δ_a values estimated from these two independent methods and they are in strong
43 agreement. This study provides an analytical framework to estimate δ_a using existing facilities,
44 and provides important insights into the traditional Keeling plot approach by showing: a) a
45 possibility to calculate the proportion of evapotranspiration fluxes to total atmospheric vapor
46 using the same instrumental setup for the traditional Keeling plot investigations, and b)
47 perspectives on estimation of isotope composition of ambient CO₂ (δ_a^{13C}).

48

49 **Key words:** HYSPLIT, intersection point, Intermediate Value Theorem, Keeling plot, stable
50 isotope

Deleted: an

52 1. Introduction

53 Stable isotopes of hydrogen and oxygen ($^1\text{H}^2\text{HO}$ and H_2^{18}O) have been widely used in
54 root water uptake source identification (Corneo et al., 2018, Mahindawansa et al., 2018,
55 Lanning et al., 2020) and evapotranspiration (ET) partitioning (Brunel et al., 1997; Wang et al.,
56 2010; Cui et al., 2020) in terrestrial ecosystems based on Craig-Gordon model (Craig and
57 Gordon, 1965), isotope mass balance and mechanisms of isotopic fractionation (Majoube, 1971;
58 Merlivat and Jouzel, 1979). With the advent of laser isotope spectrometry capable of high
59 frequency (1 Hz) measurements of the isotopic composition of atmospheric water vapor (δ_v)
60 and atmospheric water vapor content (C_v) (Kerstel and Gianfrani, 2008; Wang et al., 2009), the
61 number of studies based on high frequency ground-level isotope measurements was
62 continuously increasing. These studies generate new insights into the processes that affect δ_v ,
63 including meteorological factors (Galewsky et al., 2011; Steen-Larsen et al., 2013), biotic
64 factors (Wang et al., 2010) and multiple factors (Parkes et al., 2016). Such increase in δ_v
65 measurements allows an isotope-enabled global circulation models (Iso-GCMs) to estimate the
66 variation of water vapor isotope parameters at a global scale (Werner et al., 2011).
67 Concomitantly, more than δ_v , several new methods using high frequency ground-level isotope
68 measurements were devised to directly estimate the isotopic composition of leaf water (Song
69 et al., 2015) and leaf transpired vapor (Wang et al., 2012).

70 Evapotranspiration is a crucial component of water budget across scales such as field
71 (Wagle et al., 2020), watershed (Zhang et al., 2001), regional (Hobbins et al., 2001) and global
72 (Jung et al., 2010, Wang et al., 2014) scales. The water isotopic composition of ET (δ_{ET}) was
73 generally estimated by Keeling plot approach (Keeling, 1958). It was first used to explain

74 carbon isotope ratios of atmosphere CO₂ and to identify the sources that contribute to increases
75 in atmospheric CO₂ concentration, and has been further used to estimate δ_{ET} in recent two
76 decades (Yakir and Sternberg, 2000). Keeling plot analyses can be applied using δ_v and C_v
77 output by laser based analyzer either from different heights (Yepez et al., 2003; Zhang et al.,
78 2011; Good et al., 2012) or at one height with continuous observations (Wei et al., 2015;
79 Keppler et al., 2016). Although the intercept of the linear regression line was commonly used
80 as estimated δ_{ET} , the slope of the Keeling plot was also used to estimate δ_{ET} by re-arranging the
81 Keeling plot equations (Miller and Tans, 2003; Fiorella et al., 2018). Keeling plot approach was
82 based on isotope mass balance and two-source assumption using two equations with three
83 unknowns. As a result, the isotopic composition of other potential sources (e.g., water vapor
84 not from ET), as well as isotopic composition of ambient water vapor (δ_a), were not able to be
85 estimated directly using the Keeling plot approach. That is one of the reasons why field scale
86 moisture recycling is difficult to estimate to date.

87 In this study, we proposed two new methods to estimate δ_a , one based on the intersection
88 of two Keeling plots of two continuous observation moments and the other based on the
89 Intermediate Value Theorem. Proposition and proof were provided, and the new methods were
90 tested using field observations. As direct observations of δ_a rarely exist (Griffis et al., 2016),
91 we tested our methods by (a) making an external water vapor tracking investigation according
92 to HYSPLIT model to explain the variations of estimated δ_a , and (b) making a regression
93 analysis on daily scale and point to point scale using δ_a estimated by these two independent
94 methods.

117 this time interval, we have

118 $k_1 = C_a(\delta_a - \delta_{ET_1})$, (4)

119 $k_2 = C_a(\delta_a - \delta_{ET_2})$, (5)

120 where k_i and δ_{ET_i} represent the value at t_i for $i=1, 2$. From (4) and (5), we can solve δ_a as:

121
$$\delta_a = \frac{k_1\delta_{ET_2} - k_2\delta_{ET_1}}{k_1 - k_2}$$
 . (6)

122 ~~Algebraically, δ_a and C_a are solutions in Eq. (4) and Eq. (5). Geometrically, point $(\delta_a, 1/C_a)$ is~~
123 ~~the intersection of two Keeling plots at t_1 and t_2 . That is the reason the method was named IP~~
124 ~~method.~~ The local constant approximation idea was first described in [Yamanaka and Shimizu](#)
125 [\(2007\)](#) as an assumption to quantify the contribution of local ET to total atmospheric vapor.

126 **Intermediate Value Theorem (IVT) method.** Denote the slope as $k = C_a(\delta_a - \delta_{ET})$.

127 Since $C_a < C_v = C_a + C_{ET}$, we have $C_a = \frac{k}{(\delta_a - \delta_{ET})} < C_v$. We can rearrange $\frac{k}{(\delta_a - \delta_{ET})} < C_v$
128 to attain δ_a : $\delta_a < \frac{k}{C_v} + \delta_{ET} = \delta_v$ when $k < 0$, and $\delta_a > \frac{k}{C_v} + \delta_{ET} = \delta_v$ when $k > 0$.

129 For the smooth function $\delta_a(t)$ defined on the interval $[t_1, t_2]$ with the two time points
130 satisfying $k(t_1)k(t_2) < 0$, depending on the sign of the slopes $k(t_1)$ and $k(t_2)$ and the order
131 of $\delta_{v_1} = \delta_v(t_1)$ and $\delta_{v_2} = \delta_v(t_2)$ at the two time points t_1 and t_2 , it will correspond to one
132 of the situations in **Fig. 1**. For all of the situations, by the Intermediate Value Theorem, there
133 exists a sub-interval $[t'_1, t'_2] \subset [t_1, t_2]$ such that the whole range of $\{\delta_a(t) : t \in [t'_1, t'_2]\}$ is
134 within $[\min(\delta_{v_1}, \delta_{v_2}), \max(\delta_{v_1}, \delta_{v_2})]$. Proof details of this proposition is shown in the
135 appendix. Thus for the two nearby time points t_1 and t_2 with k_1 and k_2 having different signs, δ_a
136 will be between δ_{v_1} and δ_{v_2} . This provides a prerequisite for estimating the parameter of
137 interest δ_a based on Intermediate Value Theorem, which leads to approximation of δ_a within the
138 time interval between t_1 and t_2 using δ_{v_1} and δ_{v_2} :

- Deleted: common
- Formatted: Subscript
- Formatted: Subscript
- Deleted: P
- Deleted: in
- Deleted: why
- Formatted: Font color: Blue

- Formatted: Font: Italic
- Formatted: Font: Italic

- Formatted: Font: Italic
- Formatted: Font: Italic

143
$$\delta_a \approx \frac{\delta_{v_1} + \delta_{v_2}}{2} \quad (7)$$

144 Using this method, we are able to compute δ_a using data points when the slopes of
145 Keeling plots change signs between two adjacent time points.

146 2.2 Field observations

147 2.2.1 Study site

148 A field measurement was conducted over a maize field (39 ha) from 1st May 2017 to 30st
149 September 2017 at Shiyanghe Experimental Station of China Agricultural University, located
150 in Wuwei of Gansu Province, northwest China (37°85'N, 102°88'E; altitude 1581m). The
151 region belongs to temperate continental climate and is in the oasis within the Shiyang river
152 basin. The annual mean temperature of the study area is about 8.8°C with pan evaporation of
153 2000 mm, annual precipitation of 164.4 mm, mean sunshine duration of 3000 h, and frost-free
154 period of more than 150 d. The local crops are irrigated using groundwater with electrical
155 conductivity of 0.62 dSm⁻¹. The groundwater table is 30-40 m below the surface. Maize was
156 sowed on April and harvested on September 2017, with row spacing of 40 cm and plant spacing
157 of 23 cm. The maize growing stage was divided into seedling stage (April 21st –May 20th),
158 jointing stage (May 21st-July 10th), heading period (July 11th-July 31st), pustulation period
159 (August 1st-August 31st) and mature period (September 1st-September 20th).

160 2.2.2 Instrument setup and measurement design

161 A 24-meter flux tower, located in the middle of maize field, was used to measure ET flux
162 and isotopic composition of water vapor at different heights. The field is approximately 600 m
163 long and 240 m wide, with a 10% slope decreasing from southwest to northeast. Five gas traps
164 were installed on the flux tower at heights of 4 m, 8 m, 12 m, 16 m and 20 m, respectively. An

165 iron pillar was placed 20 m away from the flux tower. Three gas traps were installed on the iron
166 pillar, one was close to the canopy, and the other two were 2 m and 3 m above the ground.
167 Canopy gas trap was adjusted weekly according to the height of maize.

168 *In situ* δ_v and C_v collected by the eight gas traps were monitored by a water vapor isotope
169 analyzer (L2130-i, Picarro Inc., Sunnyvale, CA, USA), which was a wavelength scanned cavity
170 ring down spectroscopy (WS-CRDS) instrument. Vapor specifications include a measurement
171 range from 1000 to 50000 ppm, the precision is 0.04‰ to 0.25‰ for $\delta^{18}\text{O}$ (Zhao et al., 2019).
172 Interfacing with the gas trap and the isotope analyzer, teflon tube was wrapped by thermal
173 insulation cotton to avoid vapor condensation during transmission. The measurement of δ_v and
174 C_v were conducted from May to September, which should have 153 days of data. Forty-nine
175 days among them were complete with 24-hour continuous datasets. There were missing data
176 for either a whole day or several hours of a day for other days due to the calibration and
177 maintenance of the analyzer. These 49 days were chosen in our study for data analysis.

Deleted: 0

Formatted: Font color: Blue

178 2.2.3 Calibration of δ_v and C_v

179 Our calibration procedure mainly followed the study by Steen-Larsen et al. (2013) with
180 some modifications to fit our specific experimental setup. The water vapor from eight inlets
181 were sampled continuously over a 24-hour-period. Since only one analyzer was used to measure
182 the δ_v and C_v , the values of eight sampling inlets were recorded in turn every 225s in a 30 mins
183 cycle. The switch procedure was automatic. As the analyzer makes a measurement every 0.9-
184 1s, approximately 259-264 values for each inlet was recorded within the cycle. For each 225s
185 measurement period, No. 195 to No. 253 data points were used to avoid memory issue and
186 influence of transient pressure variation. The absolute value of coefficient of variations (|CV|)

Deleted: was

189 of δ_v and C_v were no more than 0.016 and 0.002, respectively, which was far below the critical
190 value of 15% (Lovie, 2005). The mean value of the selected data points was regarded as the
191 measured δ_v and C_v in a specific inlet. Measured C_v was used directly as actual C_v , while
192 measured δ_v was calibrated to minimize the influence of isotopic concentration dependence.
193 The C_v in our measurement ranged from 5386 ppm to 30255 ppm. Thus, C_v gradients of 10000
194 ppm, 20000 ppm and 30000 ppm were selected as calibration concentrations to improve the
195 precision of δ_v . [As we need continuous data, the observation should last uninterrupted as long](#)
196 [as possible. As a result, the calibration was made in every 5-10 days, which is consistent with](#)
197 [the frequency of calibration by other researchers such as Steen-Larsen et al. \(2013\). According](#)
198 [to our calibration data on standards, the average drift \(absolute value\) was about 0.16‰](#)
199 [between two adjacent calibrations.](#)

200 2.3 Data quality control for δ_a estimation

201 With a 30-min interval for 49 days, we should in theory produce 2352 δ_a values for both
202 IP method and IVT method. However, because of the precondition of $k_1k_2 < 0$ required for the
203 IVT method, 166 δ_a values was able to be calculated using the IVT method ($\delta_{a(IVT)}$). δ_a values
204 using the IP method ($\delta_{a(IP)}$) was not restricted by this precondition. Furthermore, a filter
205 ($\delta_{ET} < \delta_v < \delta_a$ or $\delta_{ET} > \delta_v > \delta_a$) was used for both methods because δ_v was a mixture of δ_{ET} and δ_a .
206 Therefore, δ_a values that meet both precondition $k_1k_2 < 0$ and the condition of $\delta_{ET} < \delta_v < \delta_a$ or
207 $\delta_{ET} > \delta_v > \delta_a$ were considered satisfying the criteria for the IVT method; δ_a values that meet the
208 condition of $\delta_{ET} < \delta_v < \delta_a$ or $\delta_{ET} > \delta_v > \delta_a$ were considered satisfying the criteria for the IP method.
209 In the end, we obtained 1264 and 103 δ_a values using IP and IVT methods, respectively (**Table**
210 **1**). Eighty eight time points were overlapped between the **IP** and **IVT** based δ_a results. These 88

Deleted: The calibration was made in every 5-10 days.

Deleted: $\delta_{a(IP)}$

Deleted: $\delta_{a(IVT)}$

214 time points were selected to test the reliability of two methods at point to point scale. During
215 the 49 days, there were 21 days when more than one $\delta_{a(IVT)}$ was attained for each day. These 21
216 days was also used to investigate the time series of daily scale δ_a variations and other isotopic
217 variations. Further analysis in section 2.4 in the following was made on these 21 days.

218 2.4 Explanations of δ_a using backward trajectories

219 To explain the variations of estimated δ_a , air mass backward trajectories were calculated
220 using the Hybrid Single Particle Lagrangian Integrated Trajectory (HYSPLIT) model (Draxler
221 and Hess, 1997; Draxler, 2003; Stein et al., 2015; Kaseke et al., 2018) and meteorological data
222 from the Global Data Assimilation System 0.5 Degree (GDAS0p5) with $0.5^\circ \times 0.5^\circ$ spatial
223 resolution and 3-hour time resolution for the 21 days mentioned in section 2.3. Five hundred
224 meters height was selected in the modeling. Each backward trajectory was initialized from the
225 station (37°85'N, 102°88'E) at 12:00 pm (local time), and calculated backward for 72 hours.
226 Eighteen trajectories were computed, except for June 21st, August 18th and September 29th when
227 vertical velocity data were missing. Finally, we used these 18 trajectories representing the vapor
228 origin in the corresponding 18 days.

Deleted: represented

229 3. Results

230 3.1 Time series variations of δ_{ET} , δ_v , δ_a and k

231 Time series of isotopic variations were shown in **Fig. 2**. The δ_v here is the average value
232 of eight heights. The average δ_{ET} , δ_v , $\delta_{a(IP)}$ and $\delta_{a(IVT)}$ were -11.04‰, -13.00‰, -13.60‰ and -
233 13.29‰, respectively in those 21 days when more than one $\delta_{a(IVT)}$ was attained for each day.
234 Daytime (7:00am-7:00pm) average δ_{ET} , δ_v , $\delta_{a(IP)}$ and $\delta_{a(IVT)}$ were -10.73‰, -13.33‰, -14.08‰
235 and -13.63‰, respectively. While at nighttime (7:00pm-7:00am the next day), average δ_{ET} was

237 lower than that at daytime, which was on the contrary with δ_v , $\delta_{a(IP)}$ and $\delta_{a(IVT)}$. The trend of $\delta_{a(IP)}$
238 and $\delta_{a(IVT)}$ were similar to δ_v . In majority of circumstances, δ_{ET} is the largest of those four
239 isotopic parameters, except on May 19th, June 4th and June 9th. About 76% of k values were
240 negative, and most positive k values occurred at nighttime (60%). The percentage of positive k
241 values were 33%, 34%, 24%, 34% and 10% in May, June, July, August and September,
242 respectively. Standard deviation ~~was~~ used here to evaluate the constancy among isotopic
243 parameters at daily scale. The standard deviation of δ_{ET} , δ_v , $\delta_{a(IP)}$ and $\delta_{a(IVT)}$ were 6.08‰, 0.91‰,
244 1.38‰ and 0.59‰, respectively. Therefore, the constancy of δ_a was similar to the constancy of
245 δ_v at daily scale.

Deleted: were

246 3.2 Daily variations of HYSPLIT backward trajectories and δ_a using two methods

247 The 500 m height water vapor backward trajectories revealed that water vapor was from
248 outside the study regions for ten days (**Fig. 3a**), and water vapor was from local ET for eight
249 days (**Fig. 3b**).

250 As for the IP method, 53.7% of $\delta_{a(IP)}$ values met the criteria, and 49.4% of $\delta_{a(IP)}$ values
251 meeting the criteria were during the daytime (7:00am-7:00pm). The range of $\delta_{a(IP)}$ values
252 meeting the criteria were between -16.79‰ and -12.95‰ for the ten days with external origins
253 (**Fig. 3a**). The range of $\delta_{a(IP)}$ values meeting the criteria were between -12.77‰ and -9.51‰
254 for the eight days with local origins (**Fig. 3b**).

255 As for the IVT method, only 4.4% of δ_a values met the criteria, and 35.9% of δ_a values
256 meeting the criteria were during the daytime (7:00am-7:00pm). The range of $\delta_{a(IVT)}$ values
257 meeting the criteria were between -16.31‰ and -13.93‰ for the ten days with external origins
258 (**Fig. 3a**). The range of $\delta_{a(IVT)}$ values meeting the criteria were between -12.67‰ and -9.12‰

260 for the eight days with local origins (**Fig. 3b**).

261 3.3 Linear regression between $\delta_{a(IP)}$ and $\delta_{a(IVT)}$

262 Method comparison was made at both daily scale (**Fig. 4a**) and point to point scale (**Fig.**
263 **4b**). The 21 days (see method section 2.3) in **Fig. 3a** and **Fig. 3b** were selected to figure out the
264 daily scale relationship between $\delta_{a(IP)}$ and $\delta_{a(IVT)}$. Point to point scale data was based on the 88
265 point of overlapped $\delta_{a(IP)}$ and $\delta_{a(IVT)}$ (see method section 2.3) among all 49 days, which
266 accounted for 7.0% of δ_a values using IP method and 85.4% of δ_a values using IVT method.
267 Linear regression between $\delta_{a(IP)}$ and $\delta_{a(IVT)}$ was significant at both daily scale and point to point
268 scale. The degree of agreement was less for the daily time scale than point to point scale and
269 the RMES between these two methods at daily scale and point to point scale were 0.618‰ and
270 0.167‰, respectively.

271 4. Discussion

272 4.1 The reliability of δ_a estimating methods

273 The IP method was based on the assumption that the ambient sources were the same
274 between two continuous observation moments. This is a reasonable assumption for short time
275 intervals. For the IVT method, δ_a was derived from δ_v in two continuous moments when their
276 Keeling plot slopes were opposite. The opposite slopes of the Keeling plots were the only
277 requirement. As δ_v was almost constant in two continuously moments, $\delta_{a(IVT)}$ was able to be
278 constrained into a small range. The derivation was supported by the
279 Intermediate Value Theorem. Therefore, both methods of estimating δ_a were theoretically
280 sound.

281 The δ_a results were also examined by HYSPLIT backward trajectories to identify the

282 different sources of water vapor, which assesses the reliability of both methods indirectly. Based
 283 on the trajectory analysis, water vapor in the study area came from westerlies, northern polar
 284 region and local recirculation. Water vapor from southwest monsoon and northwest Pacific
 285 were not detected in this study. Based on the isotope variation of meteoric water (Fricke et al.,
 286 1999), water vapor from westerlies and northern polar was more ¹⁸O depleted than local
 287 recycled moisture through ET. It was also reported that the water vapor from outside the study
 288 regions will lower δ_v values (Ma et al., 2014; Chen et al., 2015). The calculated δ_a values of the
 289 ten days with external sources (Fig. 3a) based on the IP method and IVT approach were lower
 290 than those of eight days with local origin (Fig. 3b), which was consistent with our expectation.
 291 The results indicate that quantifying δ_a using both the IP method and IVT approach was reliable.
 292 The reliability of two methods at point to point scale were also supported by the close
 293 relationship of δ_a using these two independent methods. Daily time scale result is less reliable
 294 than point to point scale.

Deleted: higher

295 4.2 The application of δ_a for moisture recycling

296 When δ_a was estimated, moisture recycling (e.g., f_{ET} , the contribution of ET fluxes to the
 297 total water vapor) can be estimated using the following equations with known δ_a , δ_{ET} , δ_v , C_{ET}
 298 and C_v :

$$299 \quad C_{ET} = C_v \cdot \frac{\delta_a - \delta_v}{\delta_a - \delta_{ET}}, \quad (8)$$

$$300 \quad f_{ET} = \frac{C_{ET}}{C_v}, \quad (9)$$

301 According to Eq. (8) and Eq. (9), f_{ET} was only related to δ_a , δ_v , and δ_{ET} . These three
 302 parameters were obtained for relatively small temporal and spatial scales in this study, making
 303 it possible to estimate f_{ET} at a tower scale. The f_{ET} estimate will provide a baseline value for

305 rainfall recycling ratio calculations. Previous studies quantified the contribution of recycled
306 vapor to annual or monthly precipitation in river basins using two-element mixture model (Kong
307 et al., 2013) and three-element mixture (Peng et al., 2011). At the watershed scale, recycled
308 vapor rate refers to the contributions of moisture from terrestrial ET to annual or monthly
309 precipitation (Trenberth, 1999). It is a key part of local water cycle and the atmospheric water
310 vapor balance (Seneviratne et al., 2006; Aemisegger et al., 2014). In our study, the role of f_{ET}
311 to regional vapor is similar to the role of recycled vapor rate to annual or monthly precipitation,
312 but f_{ET} was calculated with fine temporal (e.g., hourly) and spatial (i.e., field scale) scales. At
313 the watershed scale, assumption was made that no isotopic fractionation between transpiration
314 and source water (Flanagan et al., 1991); advected vapor was assumed to be the precipitation
315 vapor of the upwind station (Peng et al., 2011). However, the isotope composition of plant
316 transpired vapor is variable in a day especially under non-steady-state conditions (Farquhar and
317 Cernusak, 2005; Lai et al., 2008; Song et al., 2011). In addition, sometimes it is difficult to
318 select an upwind station without precipitation events. In this study, a field site was selected to
319 calculate the proportion of ET fluxes to total atmospheric vapor and f_{ET} was only related to δ_a ,
320 δ_v , and δ_{ET} according to Eq. (8) and Eq. (9). This indicates that f_{ET} calculations is possible for
321 fine temporal and spatial scales after estimating δ_a using the methods we proposed.

Deleted: small

322 If we assumed that the parameter δ_v in Eq. (8) is the average δ_v value measured from all
323 the eight heights. f_{ET} in this study was 23.3% and 12.7% from May to September 2017 based
324 on daily $\delta_{a(IP)}$ and daily $\delta_{a(TVT)}$, respectively. It was reported that recycled vapor rate in all
325 Shiyang river basin, oasis region, mountain region and desert region were 23%, 28%, 17% and
326 15%, respectively (Li, et al., 2016; Zhu, et al., 2019). The f_{ET} based on daily $\delta_{a(IP)}$ in our study

Deleted: in

Deleted: and

330 was close to these earlier studies. The deviation of f_{ET} based on daily $\delta_{a(IVT)}$ from previous
331 studies may be because 64.1% of point to point $\delta_{a(IVT)}$ was observed at nighttime. Normally, ET
332 at nighttime is lower than that of daytime. f_{ET} may be underestimated using daily $\delta_{a(IVT)}$. It could
333 also be inferred that f_{ET} estimation using Eq. (9) may be more reliable using daily $\delta_{a(IP)}$ than
334 daily $\delta_{a(IVT)}$.

Deleted: compared with

335 4.3 Implications of δ_a

336 The signature of δ_E and δ_T was first introduced by a hypothetical graph shown on **Fig.**
337 **5a** (Moreira et al., 1997). Line 1 and line 2 was idealized Keeling plot with pure T and pure E,
338 and Line 3 was the Keeling plot with mixed T and E. The IVT method in this study provided a
339 general explanation of this figure. As T is a major component of ET in the daytime in non-arid
340 region (Wang et al., 2014), the slope is generally negative. When E dominates ET in an
341 ecosystem, such as in the nighttime in non-arid region or in arid region, the slope should be
342 positive. Mathematically, negative slope is due to $\delta_{ET} > \delta_a$ and positive slope is due to $\delta_{ET} < \delta_a$.

Deleted: <

Deleted: >

343 It also reflected that IVT method could only be used in non-arid ecosystems to ensure the
344 occurrence of sign switch (e.g., from negative to positive) in Keeling plot slopes. On the
345 contrary, IP method may not be restricted by the type of ecosystems. Yamanaka and Shimizu
346 (2007) used the assumption that δ_a of an area of 219.9 km² was represented by the intersection
347 point of two Keeling plot lines in different sites with synchronous measurements and they used
348 the intersection value as an approximate value of δ_a . This study was conducted in a maize field
349 using 30-min interval measurements. The results verified Yamanaka and Shimizu's (2007)
350 assumption in such fine spatial and temporal scale, and indicate that accurate $\delta_{a(IP)}$ could be
351 estimated from the intersection of two Keeling plots regardless the slope being positive or

Deleted: appearance

Deleted: transfer plus or minus in

Deleted: s²

358 negative, while the $\delta_{a(IVT)}$ should be restricted in the area between two dotted lines as shown in
359 **Fig. 5b** (i.e., between the minimum value of δ_v in positive slope and the maximum value of δ_v
360 in negative slope). Although IVT method relies on more stringent precondition for data filtering,
361 this method requires a very simple expression, which only needs two parameters to be measured
362 according to Eq. (7).

363 While this study is about water vapor ^{18}O , the “Keeling plot” was first used by Keeling
364 (1958, 1961) to interpret carbon isotope ratios of mixed CO_2 and to identify the sources that
365 contribute to increases in atmospheric CO_2 concentrations on a regional basis. Compared with
366 ET in water vapor which consists of E and T, net ecosystem CO_2 exchange is comprised of soil
367 respiration (R) and gross primary productivity (GPP). As $^{13}\text{CO}_2$ isotopic Keeling plot reveals a
368 positive slope during both daytime and nighttime (Yakir and Wang, 1996; Unger et al., 2010),
369 the IVT method may not be able to estimate ambient $^{13}\text{CO}_2$ isotopic composition ($\delta_a^{13}\text{C}$) since
370 there are no opposite slopes in a day. In such case, the IP method may be implemented in two
371 continuous moments to estimate $\delta_a^{13}\text{C}$ and may consequently further calculate the contribution
372 of NEE to atmospheric CO_2 .

373 5. Conclusions

374 In this study, we established two methods to quantify δ_a using intersection point method
375 and the Intermediate Value Theorem method. The IVT method was used under the condition of
376 opposite slope of Keeling plots in two continuously moments. The results of estimated $\delta_{a(IP)}$ and
377 $\delta_{a(IVT)}$ were consistent with the expectation whether it was local origin or external origin using
378 external vapor tracking investigation by HYSPLIT model. The linear regression between $\delta_{a(IP)}$
379 and $\delta_{a(IVT)}$ was highly significant at both daily time scale and point to point scale.

Deleted: (

Deleted: ,

Deleted: both on

383 This study provided insights into the underexplored traditional Keeling plots and
384 provided two methods to estimate δ_a using the same instrumental setup for the traditional
385 Keeling plot investigations. The estimated δ_a will make it possible to calculate the ET
386 contribution to regional vapor at a 30 min interval at field scale. The results [also](#) indicate that
387 using similar framework, δ_a^{13C} may also solvable by the IP method.

388 6. Acknowledgements

389 We acknowledge support from the National Natural Science Foundation of China
390 (51725904, 51621061, 51861125103), the National Key Research Program
391 (2016YFC0400207), the Discipline Innovative Engineering Plan (111 Program, B14002), [the](#)
392 [Graduate International Training and Promotion Program of China Agricultural University](#)
393 [\(31051521\)](#), and the President's International Research Awards from Indiana University and
394 the Division of Earth Sciences of National Science Foundation (EAR-1554894). We thank Dr.
395 Qianning Liu from Jiangxi University of Finance and Economics and Dr. Zhengxiang Chen
396 from Capital Normal University for checking the validity of the Intermediate Value Theorem
397 method.

398 7. Code and Data availability

399 Code and data are available on request.

400 8. Author contribution

401 YY, TD and LW conceptualized the main research questions. YY collected data
402 and performed the data analyses. YY and LW wrote the first draft. HW contributed to
403 additional data analyses. All the authors contributed ideas and edited the manuscript.

404 9. Competing interests

405 There authors declare no competing interests.

406 10. References

- 407 Aemisegger, F., Pfahl, S., Sodemann, H., Lehner, I., Seneviratne, S. I., and Wernli, H.:
408 Deuterium excess as a proxy for continental moisture recycling and plant transpiration,
409 **Atmospheric Chemistry and Physics**, 14, 4029–4054, doi: 10.5194/acp-144029-2014, 2014.
- 410 Brunel, J. P., Walker, G. R., Dighton, J. C., and Monteny, B.: Use of stable isotopes of water to
411 determine the origin of water used by the vegetation and to partition evapotranspiration. A
412 case study from HAPEX-Sahel, **Journal of Hydrology**, 188–189, 466–481,
413 doi:10.1016/s0022-1694(96)03188-5, 1997.
- 414 Chen, F. L., Zhang, M. J., Ma, Q., Wang, S. J., Li, X. F., and Zhu, X. F.: Stable isotopic
415 characteristics of precipitation in Lanzhou city and its surrounding areas, Northwest China,
416 **Environmental Earth Sciences**, 73, 4671–4680, doi: 10.1007/s12665-014-3776-6, 2015.
- 417 Comeo, P. E., Kertesz, M. A., Bakhshandeh, S., Tahaei, H., Barbour, M. M., and Dijkstra, F. A.:
418 Studying root water uptake of wheat genotypes in different soils using water $\delta^{18}\text{O}$ stable
419 isotopes, **Agriculture, Ecosystems & Environment**, 264, 119-129, doi:
420 10.1016/j.agee.2018.05.007, 2018.
- 421 Craig, H. and Gordon, L. I.: Deuterium and oxygen 18 variations in the ocean and marine
422 atmosphere, in: **Stable Isotopes in Oceanographic Studies and Paleotemperatures**, p. 9,
423 1965.
- 424 Cui, J., Tian, L., Wei, Z., Huntingford, C., Wang, P., Cai, Z., Ma, N., and Wang, L.: Quantifying
425 the controls on evapotranspiration partitioning in the highest alpine meadow ecosystems,
426 **Water Resources Research**, 56, doi: 10.1029/2019WR024815, 2020.
- 427 Draxler, R. R., and Hess, G.: Description of the HYSPLIT4 modeling system, **NOAA Tech**
428 **Memo ERL ARL-224**, Dec, 24p., 1997.
- 429 Draxler, R. R.: Evaluation of an ensemble dispersion calculation, **Journal of Applied**
430 **Meteorology**, 42, 308-317, doi: 10.1175/1520-0450(2003)042<0308:EOAEDC>2.0.CO;2,
431 2003.
- 432 Farquhar, G. D., and Cernusak, L. A.: On the isotopic composition of leaf water in the non-
433 steady state, **Functional Plant Biology**, 32(4), 293-303, doi: 10.1071/FP04232, 2005.
- 434 Fiorella, R. P., Poulsen, C. J., and Matheny, A. M.: Seasonal patterns of water cycling in a deep,
435 continental mountain valley inferred from stable water vapor isotopes, **Journal of**
436 **Geophysical Research: Atmospheres**, 123, 7271-7291, doi: 10.1029/2017JD028093, 2018.
- 437 Flanagan, L. B., Comstock, J. P., and Ehleringer, J. R.: Comparison of modeled and observed
438 environmental influences on the stable oxygen and hydrogen isotope composition of leaf
439 water in *Phaseolus vulgaris* L, **Plant Physiology**, 96, 588-596, doi:
440 <https://doi.org/10.1104/pp.96.2.588>, 1991.
- 441 Fricke, H. C., O'Neil, J. R. J. E., and Letters, P. S.: The correlation between $^{18}\text{O}/^{16}\text{O}$ ratios of
442 meteoric water and surface temperature: its use in investigating terrestrial climate change over
443 geologic time, **Earth and Planetary Science Letters**, 170, 181-196, doi: 10.1016/S0012-
444 821X(99)00105-3, 1999.

445 Galewsky, J., Rella, C., Sharp, Z., Samuels, K., and Ward, D.: Surface measurements of upper
446 tropospheric water vapor isotopic composition on the Chajnantor Plateau, Chile, **Geophysical**
447 **Research Letters**, 38, 1-5, doi: 10.1029/2011GL048557, 2011.

448 Good, S. P., Soderberg, K., Wang, L., and Caylor, K. K.: Uncertainties in the assessment of the
449 isotopic composition of surface fluxes: A direct comparison of techniques using laser-based
450 water vapor isotope analyzers, **Journal of Geophysical Research: Atmospheres**, 117, doi:
451 10.1029/2011JD017168, 2012.

452 Griffis, T. J., Wood, J. D., Baker, J. M., Lee, X., Xiao, K., Chen, Z., Welp, L. R., Schultz, N. M.,
453 Gorski, G., and Chen, M.: Investigating the source, transport, and isotope composition of
454 water vapor in the planetary boundary layer, **Atmospheric Chemistry and Physics**, 16,
455 5139-5157, doi: 10.5194/acp-16-5139-2016, 2016.

456 Hobbins, M. T., Ramirez, J. A., and Brown, T. C.: The complementary relationship in estimation
457 of regional evapotranspiration: An enhanced advection-aridity model, **Water Resources**
458 **Research**, 37, 1389-1403, doi: 10.1029/2000WR900359, 2001.

459 Jung, M., Reichstein, M., Ciais, P., Seneviratne, S. I., Sheffield, J., Goulden, M. L., Bonan, G.,
460 Cescatti, A., Chen, J., and De Jeu, R.: Recent decline in the global land evapotranspiration
461 trend due to limited moisture supply, **Nature**, 467, 951-954, doi: 10.1038/nature09396, 2010.

462 Kaseke, K. F., Wang, L., Wanke, H., Tian, C., Lanning, M., and Jiao, W.: Precipitation origins
463 and key drivers of precipitation isotope (^{18}O , ^2H , and ^{17}O) compositions over windhoek,
464 **Journal of Geophysical Research: Atmospheres**, 123, 7311-7330, doi:
465 10.1029/2018JD028470, 2018.

466 Keeling, C. D.: The concentration and isotopic abundances of atmospheric carbon dioxide in
467 rural areas, **Geochimica et Cosmochimica Acta**, 13, 322-334, doi: 10.1016/0016-
468 7037(58)90033-4, 1958.

469 Keeling, C. D.: The concentration and isotopic abundances of carbon dioxide in rural and marine
470 air, **Geochimica et Cosmochimica Acta**, 24, 277-298, doi: 10.1016/0016-7037(61)90023-0,
471 1961.

472 Keppler, F., Schiller, A., Ehehalt, R., Greule, M., Hartmann, J., and Polag, D.: Stable isotope and
473 high precision concentration measurements confirm that all humans produce and exhale
474 methane, **Journal of Breath Research**, 10, 016003, doi: 10.1088/1752-7155/10/1/016003,
475 2016.

476 Kerstel, E., and Gianfrani, L.: Advances in laser-based isotope ratio measurements: selected
477 applications, **Applied Physics B**, 92, 439-449, doi: 10.1007/s00340-008-3128-x, 2008.

478 Kong, Y., Pang, Z., and Froehlich, K.: Quantifying recycled moisture fraction in precipitation of
479 an arid region using deuterium excess, **Tellus B: Chemical and Physical Meteorology**, 65,
480 19251, doi: 10.3402/tellusb.v65i0.19251, 2013.

481 Lai, C. T., Ometto, J. P., Berry, J. A., Martinelli, L. A., Domingues, T. F., and Ehleringer, J. R.:
482 Life form-specific variations in leaf water oxygen-18 enrichment in Amazonian vegetation,
483 **Oecologia**, 157, 197-210, doi: 10.1007/s00442-008-1071-5, 2008.

484 Lanning, M., Wang, L., Benson, M., Zhang, Q., and Novick, K. A.: Canopy isotopic
485 investigation reveals different water uptake dynamics of maples and oaks, **Phytochemistry**,
486 175, 112389, doi:10.1016/j.phytochem.2020.112389, 2020.

487 Li, Z., Feng, Q., Wang, Q., Kong, Y., Chen, A., Song, Y., Li, Y., Li, J., and Guo, X.:
488 Contributions of local terrestrial evaporation and transpiration to precipitation using $\delta^{18}\text{O}$ and

489 D-excess as a proxy in Shiyang inland river basin in China, **Global and Planetary Change**,
490 146, 140-151, doi: 10.1016/j.gloplacha.2016.10.003, 2016.

491 Lovie, P.: Coefficient of variation, **Encyclopedia of Statistics in Behavioral Science**, doi:
492 10.1002/0470013192.bsa107, 2005.

493 Ma, Q., Zhang, M., Wang, S., Wang, Q., Liu, W., Li, F., and Chen, F.: An investigation of
494 moisture sources and secondary evaporation in Lanzhou, Northwest China, **Environmental**
495 **Earth Sciences**, 71, 3375-3385, doi: 10.1007/s12665-013-2728-x, 2014.

496 Mahindawansa, A., Orłowski, N., Kraft, P., Rothfuss, Y., Racela, H., and Breuer, L.:
497 Quantification of plant water uptake by water stable isotopes in rice paddy systems, **Plant**
498 **and Soil**, 429, 281-302, doi: 10.1007/s11104-018-3693-7, 2018.

499 Majoube, M.: Fractionnement en oxygene 18 et en deuterium entre l'eau et sa vapeur, **Journal**
500 **de Chimie Physique**, 68, 1423-1436, doi: 10.1051/jcp/1971681423, 1971.

501 Merlivat, L., and Jouzel, J.: Global climatic interpretation of the deuterium-oxygen 18
502 relationship for precipitation, **Journal of Geophysical Research: Oceans**, 84, 5029-5033,
503 doi: 10.1029/JC084iC08p05029, 1979.

504 Miller, J. B., and Tans, P. P.: Calculating isotopic fractionation from atmospheric measurements
505 at various scales, **Tellus B**, 55, 207-214, doi: 10.1034/j.1600-0889.2003.00020.x, 2003.

506 Moreira, M., Sternberg, L., Martinelli, L., Victoria, R., Barbosa, E., Bonates, L., and Nepstad,
507 D.: Contribution of transpiration to forest ambient vapour based on isotopic measurements,
508 **Global Change Biology**, 3, 439-450, doi: 10.1046/j.1365-2486.1997.00082.x, 1997.

509 Parkes, S., McCabe, M., Griffiths, A. D., Wang, L., Chambers, S., Ershadi, A., Williams, A. G.,
510 Strauss, J., and Element, A.: Response of water vapour D-excess to land-atmosphere
511 interactions in a semi-arid environment, **Hydrology and Earth System Sciences**, 21, 533-548,
512 doi:10.5194/hess-21-533-2017, 2016.

513 Peng, T. R., Liu, K. K., Wang, C. H., and Chuang, K. H.: A water isotope approach to assessing
514 moisture recycling in the island-based precipitation of Taiwan: A case study in the western
515 Pacific, **Water Resources Research**, 47, W08507, doi: 10.1029/2010WR009890, 2011.

516 Seneviratne, S. I., Lüthi, D., Litschi, M., and Schär, C.: Land-atmosphere coupling and climate
517 change in Europe, **Nature**, 443, 205-209, doi: 10.1038/nature05095, 2006.

518 Song, X., Barbour, M. M., Saurer, M., and Helliker, B. R.: Examining the large-scale
519 convergence of photosynthesis-weighted tree leaf temperatures through stable oxygen isotope
520 analysis of multiple data sets, **New Phytologist**, 192: 912-924, doi: 10.1111/j.1469-
521 8137.2011.03851.x, 2011.

522 Song, X., Simonin, K. A., Loucos, K. E., and Barbour, M. M.: Modelling non-steady-state
523 isotope enrichment of leaf water in a gas-exchange cuvette environment, **Plant, Cell &**
524 **Environment**, 38, 2618-2628, doi: 10.1111/pce.12571, 2015.

525 Steen-Larsen, H. C., Johnsen, S. J., Masson-Delmotte, V., Stenni, B., Risi, C., Sodemann, H.,
526 Balslev-Clausen, D., Blunier, T., Dahl-Jensen, D., and Ellehøj, M. D.: Continuous monitoring
527 of summer surface water vapor isotopic composition above the Greenland Ice Sheet,
528 **Atmospheric Chemistry and Physics**, 13, 4815-4828, doi:10.5194/acp-13-4815-2013, 2013.

529 Stein, A., Draxler, R. R., Rolph, G. D., Stunder, B. J., Cohen, M., and Ngan, F.: NOAA's
530 HYSPLIT atmospheric transport and dispersion modeling system, **Bulletin of the American**
531 **Meteorological Society**, 96, 2059-2077, doi: 10.1175/BAMS-D-14-00110.1, 2015.

532 Trenberth, K. E.: Atmospheric moisture recycling: Role of advection and local evaporation,

533 **Journal of Climate**, 12, 1368-1381, doi: 10.1175/15200442(1999)012<1368:AMRROA>2.0.
534 CO;2, 1999.

535 Unger, S., Máguas, C., Pereira, J. S., Aires, L. M., David, T. S., and Werner, C.: Disentangling
536 drought-induced variation in ecosystem and soil respiration using stable carbon isotopes,
537 **Oecologia**, 163, 1043-1057, doi: 10.1007/s00442-010-1576-6, 2010.

538 Wagle, P., Skaggs, T. H., Gowda, P. H., Northup, B. K., and Neel, J. P.: Flux variance similarity-
539 based partitioning of evapotranspiration over a rainfed alfalfa field using high frequency eddy
540 covariance data, **Agricultural and Forest Meteorology**, 285, 107907, doi:
541 10.1016/j.agrformet.2020.107907, 2020.

542 Wang, L., Caylor, K. K., and Dragoni, D.: On the calibration of continuous, high-precision $\delta^{18}\text{O}$
543 and $\delta^2\text{H}$ measurements using an off-axis integrated cavity output spectrometer, **Rapid**
544 **Communications in Mass Spectrometry**, 23, 530-536, doi: 10.1002/rcm.3905, 2009.

545 Wang, L., Caylor, K. K., Villegas, J. C., Barron-Gafford, G. A., Breshears, D. D., and Huxman,
546 T. E.: Partitioning evapotranspiration across gradients of woody plant cover: Assessment of a
547 stable isotope technique, **Geophysical Research Letters**, 37, L09401, doi:
548 10.1029/2010GL043228, 2010.

549 Wang, L., Good, S. P., Caylor, K. K., and Cernusak, L. A.: Direct quantification of leaf
550 transpiration isotopic composition, **Agricultural and Forest Meteorology**, 154-155, 127-
551 135, doi: 10.1016/j.agrformet.2011.10.018, 2012.

552 Wang, L., Niu, S., Good, S. P., Soderberg, K., McCabe, M. F., Sherry, R. A., Luo, Y., Zhou, X.,
553 Xia, J., and Caylor, K. K.: The effect of warming on grassland evapotranspiration partitioning
554 using laser-based isotope monitoring techniques, **Geochimica et Cosmochimica Acta**, 111,
555 28-38, doi: 10.1016/j.gca.2012.12.047, 2013.

556 Wang, L., Good, S. P., and Caylor, K. K.: Global synthesis of vegetation control on
557 evapotranspiration partitioning, **Geophysical Research Letters**, 41, 6753–6757,
558 10.1002/2014GL061439, 2014.

559 Wei, Z., Yoshimura, K., Okazaki, A., Kim, W., Liu, Z., and Yokoi, M.: Partitioning of
560 evapotranspiration using high-frequency water vapor isotopic measurement over a rice paddy
561 field, **Water Resources Research**, 51, 3716-3729, doi: 10.1002/2014WR016737, 2015.

562 Werner, M., Langebroek, P. M., Carlsen, T., Herold, M., and Lohmann, G.: Stable water isotopes
563 in the ECHAM5 general circulation model: Toward high-resolution isotope modeling on a
564 global scale, **Journal of Geophysical Research: Atmospheres**, 116, D15109,
565 doi:10.1029/2011JD015681, 2011.

566 Yakir, D., and Wang, X.F.: Fluxes of CO_2 and water between terrestrial vegetation and the
567 atmosphere estimated from isotope measurements, **Nature**, 380, 515-517, doi:
568 10.1038/380515a0, 1996.

569 Yakir, D., and Sternberg, L.: The use of stable isotopes to study ecosystem gas exchange,
570 **Oecologia**, 123, 297-311, doi: 10.1007/s004420051016, 2000.

571 Yamanaka, T., and Shimizu, R.: Spatial distribution of deuterium in atmospheric water vapor:
572 Diagnosing sources and the mixing of atmospheric moisture, **Geochimica et Cosmochimica**
573 **Acta**, 71, 3162-3169, doi: 10.1016/j.gca.2007.04.014, 2007.

574 Yepez, E. A., Williams, D. G., Scott, R. L., and Lin, G.: Partitioning overstory and understory
575 evapotranspiration in a semiarid savanna woodland from the isotopic composition of water
576 vapor, **Agricultural and Forest Meteorology**, 119, 53-68, doi: 10.1016/S0168-

577 1923(03)00116-3, 2003.
578 Zhang, L., Dawes, W., and Walker, G.: Response of mean annual evapotranspiration to
579 vegetation changes at catchment scale, **Water Resources Research**, 37, 701-708, doi:
580 10.1029/2000WR900325, 2001.
581 Zhang, Y., Shen, Y., Sun, H., and Gates, J. B.: Evapotranspiration and its partitioning in an
582 irrigated winter wheat field: A combined isotopic and micrometeorologic approach, **Journal**
583 **of Hydrology**, 408, 203-211, doi: 10.1016/j.jhydrol.2011.07.036, 2011.
584 Zhao, L., Liu, X., Wang, N., Kong, Y., Song, Y., He, Z., Liu, Q., and Wang, L.: Contribution of
585 recycled moisture to local precipitation in the inland Heihe River Basin, **Agricultural and**
586 **Forest Meteorology**, 271, 316-335, doi: 10.1016/j.agrformet.2019.03.014, 2019.
587 Zhu, G., Guo, H., Qin, D., Pan, H., Zhang, Y., Jia, W., and Ma, X.: Contribution of recycled
588 moisture to precipitation in the monsoon marginal zone: Estimate based on stable isotope
589 data, **Journal of Hydrology**, 569, 423-435, doi: 10.1016/j.jhydrol.2018.12.014, 2019.
590

591 11. Appendix

592 **Proposition.** In the traditional linear Keeling plot system, denote $\delta_a = f(t)$, $\delta_v = g(t)$,
593 $\delta_{ET} = h(t)$ and $C_a = I(t) > 0$ as continuous functions of time. And for two definite
594 moments t_1 and t_2 ($t_1 < t_2$), $\delta_{a_1} \neq \delta_{a_2} \neq \delta_{v_1} \neq \delta_{v_2} \neq \delta_{ET_1} \neq \delta_{ET_2}$. The slopes of
595 corresponding keeling plot curve are $k_1 = C_{a_1}(\delta_{a_1} - \delta_{ET_1})$ and $k_2 = C_{a_2}(\delta_{a_2} - \delta_{ET_2})$,
596 respectively. Then we have that when $k_1 k_2 < 0$, there exists $[t_1', t_2'] \subset [t_1, t_2]$, such that
597 $[\min(f(t_1'), f(t_2')), \max(f(t_1'), f(t_2'))] \subset [\min(\delta_{v_1}, \delta_{v_2}), \max(\delta_{v_1}, \delta_{v_2})]$.

598 **Remark:** To make a proof of the proposition, classical Intermediate Value Theorem (IVT)
599 was used. It states that if f is a continuous function from the interval $I = [a, b]$ to real number
600 (\mathbb{R}) . Then *Version I*. if u is a number between $f(a)$ and $f(b)$, there is c in (a, b) such that $f(c) =$
601 u . *Version II*. the image set $f(I)$ is also an interval, and it contains
602 $[\min(f(a), f(b)), \max(f(a), f(b))]$. While in this study, IVT was able to be explained as
603 follows: if f is a continuous function from the interval $I = [t_1, t_2]$ to \mathbb{R} with
604 $\min[f(t_1), f(t_2)] < \delta_v$ and $\max[f(t_1), f(t_2)] > \delta_v$, then *Version I* implies that there is t'
605 $\in (t_1, t_2)$ such that $f(t') = \delta_v$. And *Version II* implies that the image set $f(I)$ is also an

606 interval, and it contains $[\min(f(t_1), f(t_2)), \max(f(t_1), f(t_2))]$.

607 **Proof.** Since $k_1 k_2 < 0$, we have $\delta_{a_1} < \delta_{v_1}$ and $\delta_{a_2} > \delta_{v_2}$, or $\delta_{a_1} > \delta_{v_1}$ and $\delta_{a_2} <$
608 δ_{v_2} . As a result, the cases $\delta_{a_1} < \delta_{v_1} < \delta_{a_2} < \delta_{v_2}$, $\delta_{v_1} < \delta_{a_1} < \delta_{v_2} < \delta_{a_2}$, $\delta_{v_2} < \delta_{a_2} <$
609 $\delta_{v_1} < \delta_{a_1}$, $\delta_{a_2} < \delta_{v_2} < \delta_{a_1} < \delta_{v_1}$ and $[\min(\delta_{v_1}, \delta_{v_2}), \max(\delta_{v_1}, \delta_{v_2})] \cap$
610 $[\min(\delta_{a_1}, \delta_{a_2}), \max(\delta_{a_1}, \delta_{a_2})] = \emptyset$ do not meet the precondition $k_1 k_2 < 0$. There are only
611 four cases below. We will prove the proposition in each of the four cases.

612 Case 1: $[\min(\delta_{v_1}, \delta_{v_2}), \max(\delta_{v_1}, \delta_{v_2})] \subset [\min(\delta_{a_1}, \delta_{a_2}), \max(\delta_{a_1}, \delta_{a_2})]$ (**Fig. 1 a**).

613 According to IVT *Version I*, there exists $t_1' \in [t_1, t_2]$, such that $f(t_1') = \delta_{v_1}$;
614 similarly, there exists $t_2' \in [t_1, t_2]$, such that $f(t_2') = \delta_{v_2}$. Based on IVT *Version II*, there
615 exists $[t_1', t_2'] \subset [t_1, t_2]$, such that $[\min(f(t_1'), f(t_2')), \max(f(t_1'), f(t_2'))] =$
616 $[\min(\delta_{v_1}, \delta_{v_2}), \max(\delta_{v_1}, \delta_{v_2})]$.

617 Case 2: $[\min(\delta_{a_1}, \delta_{a_2}), \max(\delta_{a_1}, \delta_{a_2})] \subset [\min(\delta_{v_1}, \delta_{v_2}), \max(\delta_{v_1}, \delta_{v_2})]$ (**Fig. 1 b**).

618 According to IVT *Version I*, there exists $t_1' \in [t_1, t_2]$, such that $f(t_1') = \delta_{a_1}$;
619 similarly, there exists $t_2' \in [t_1, t_2]$, such that $f(t_2') = \delta_{a_2}$. Based on IVT *Version II*, there
620 exists $[t_1', t_2'] \subset [t_1, t_2]$, such that $[\min(f(t_1'), f(t_2')), \max(f(t_1'), f(t_2'))] =$
621 $[\min(\delta_{a_1}, \delta_{a_2}), \max(\delta_{a_1}, \delta_{a_2})] \subset [\min(\delta_{v_1}, \delta_{v_2}), \max(\delta_{v_1}, \delta_{v_2})]$.

622 Case 3: $\delta_{v_2} < \delta_{a_1} < \delta_{v_1} < \delta_{a_2}$, or $\delta_{a_2} < \delta_{v_1} < \delta_{a_1} < \delta_{v_2}$ (**Fig. 1 c and Fig. 1 d**).

623 According to IVT *Version I*, there exists $t_2' \in [t_1, t_2]$, such that $f(t_2') = \delta_{v_1}$.
624 Given case (2), when $[\min(\delta_{a_1}, \delta_{v_1}), \max(\delta_{a_1}, \delta_{v_1})] \subset [\min(\delta_{v_1}, \delta_{v_2}), \max(\delta_{v_1}, \delta_{v_2})]$, there
625 exists $[t_1', t_2'] \subset [t_1, t_2]$, such that $[\min(f(t_1'), f(t_2')), \max(f(t_1')$
626 $), f(t_2'))] \subset [\min(\delta_{a_1}, \delta_{v_1}), \max(\delta_{a_1}, \delta_{v_1})] \subset [\min(\delta_{v_1}, \delta_{v_2}), \max(\delta_{v_1}, \delta_{v_2})]$.

627 Case 4: $\delta_{v_1} < \delta_{a_2} < \delta_{v_2} < \delta_{a_1}$, or $\delta_{a_1} < \delta_{v_2} < \delta_{a_2} < \delta_{v_1}$ (**Fig. 1 e and Fig. 1 f**).

628 According to IVT Version I, there exists $t_1' \in [t_1, t_2]$, such that $f(t_1') = \delta_{v_2}$. Based
 629 on case (2), when $[\min(\delta_{a_2}, \delta_{v_2}), \max(\delta_{a_2}, \delta_{v_2})] \subset [\min(\delta_{v_1}, \delta_{v_2}), \max(\delta_{v_1}, \delta_{v_2})]$, there
 630 exists $[t_1', t_2'] \subset [t_1', t_2] \subset [t_1, t_2]$, such that $[\min(f(t_1'), f(t_2')), \max(f(t_1'$
 631 $), f(t_2'))] \subset [\min(\delta_{a_2}, \delta_{v_2}), \max(\delta_{a_2}, \delta_{v_2})] \subset [\min(\delta_{v_1}, \delta_{v_2}), \max(\delta_{v_1}, \delta_{v_2})]$.

632 Thus the proposition is true for all four possible scenarios, which make the estimation of
 633 δ_a theoretically feasibly when $k_1 k_2 < 0$ and δ_{v_1} and δ_{v_2} adequately close. Actual δ_a
 634 between t_1 and t_2 can be ensured in the interval $[\min(\delta_{v_1}, \delta_{v_2}), \max(\delta_{v_1}, \delta_{v_2})]$.
 635 To simplify the result, actual δ_a between t_1 and t_2 can be approximately regarded as what Eq. (7)
 636 reveals.

637

638

639

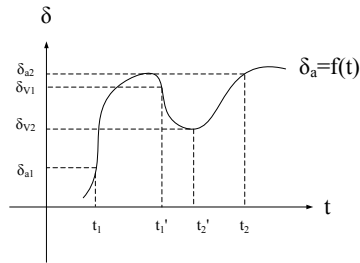
640

641

642 Table 1. The number of estimated isotope composition of ambient vapor meeting the criteria
 643 using the intersection point method ($\delta_{a(IP)}$) and the Intermediate Value Theorem method ($\delta_{a(IVT)}$)
 644 among all 49 days.

Date	number of $\delta_{a(IP)}$ values	number of $\delta_{a(IVT)}$ values
	meeting the criteria in a whole day	meeting the criteria in a whole day
5/19	27	8
5/27	13	3
5/28	30	3
5/31	25	5
6/4	38	5
6/5	28	0
6/7	29	6
6/9	32	5
6/10	26	2
6/11	21	4
6/12	22	4
6/15	32	0
6/16	33	0
6/17	24	1
6/18	26	0
6/21	26	3
6/22	22	0
6/26	22	0
6/27	29	3
7/4	23	0
7/5	23	1
7/7	30	0
7/8	29	0
7/14	28	4
7/16	28	0
7/18	25	1
7/19	28	6
7/20	27	6
7/21	29	0
7/22	19	0
8/3	18	1
8/4	22	3
8/5	25	3
8/6	28	1
8/12	13	8
8/18	19	3
8/19	30	0
8/28	23	0
8/29	22	1
8/30	27	1
8/31	27	0
9/20	25	0
9/21	24	1
9/22	31	1
9/23	28	1
9/27	28	2
9/28	25	1
9/29	30	5
9/30	25	1

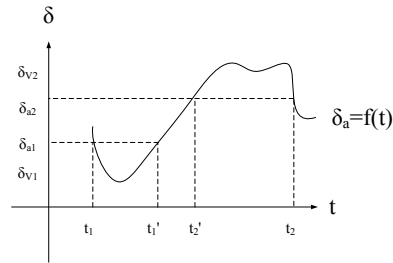
645



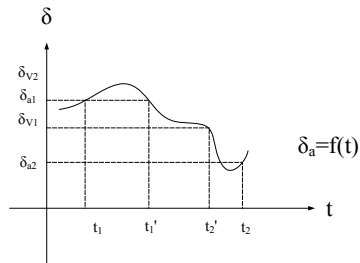
646

647

(a)



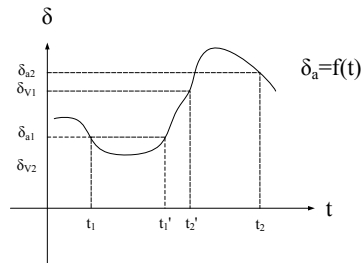
(b)



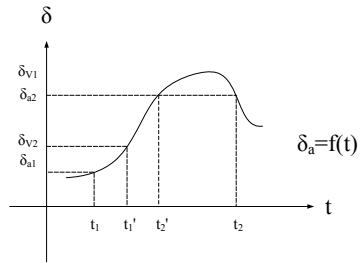
648

649

(c)



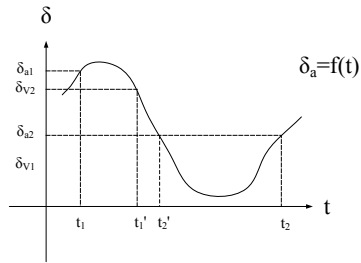
(d)



650

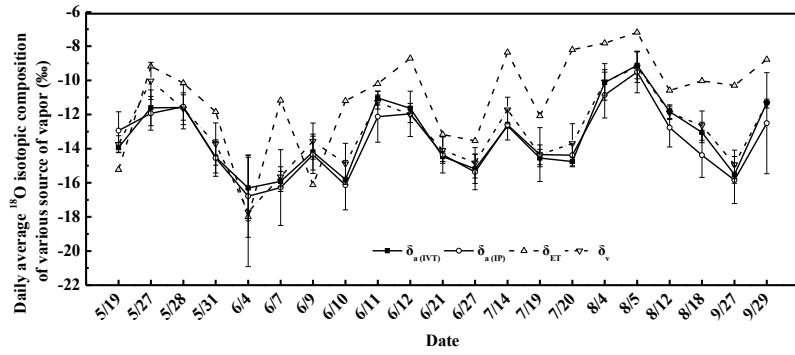
651

(e)



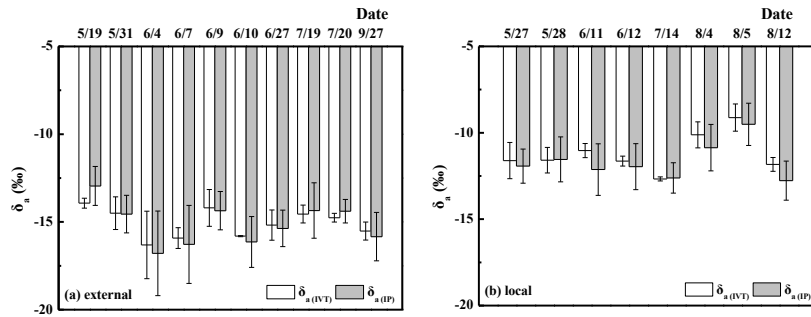
(f)

652 Fig. 1 Theoretical diagrams of all possible combinations of the relationships between isotope
 653 composition of ambient vapor (δ_a) and observed isotope composition of atmospheric vapor (δ_v)
 654 of two continuous moments t_1 and t_2 , ($t_1 < t_2$). δ_{a1} and δ_{a2} represent δ_a value in t_1 and t_2 ,
 655 respectively. δ_{v1} and δ_{v2} represent δ_v value in t_1 and t_2 , respectively. t_1' and t_2' represent the time
 656 of two specific moments between t_1 and t_2 with $t_1 < t_1' < t_2' < t_2$. For all of the six situations,
 657 there exists some sub-intervals $[t_1', t_2'] \subset [t_1, t_2]$ such that the whole range of $\{\delta_a(t) : t \in$
 658 $[t_1', t_2']\}$ is within $[\min(\delta_{v1}, \delta_{v2}), \max(\delta_{v1}, \delta_{v2})]$.
 659



660
 661 Fig. 2 The daily average values of the isotope composition of evapotranspiration vapor (δ_{ET}),
 662 the isotope composition of atmospheric vapor (δ_v), the estimated isotope composition of
 663 ambient vapor using the intersection point method ($\delta_{a(IP)}$) and the Intermediate Value Theorem
 664 method ($\delta_{a(IVT)}$) in the 21 days (see method section 2.3).
 665

666



667

668 Fig. 3 The daily average values of the estimated isotope composition of ambient vapor using
669 the intersection point method ($\delta_{a(IPT)}$) and the Intermediate Value Theorem method ($\delta_{a(IVT)}$) after
670 filter. Hybrid Single Particle Lagrangian Integrated Trajectory (HYSPPLIT) backward trajectory
671 showed external origin (a) and local origin (b), respectively.

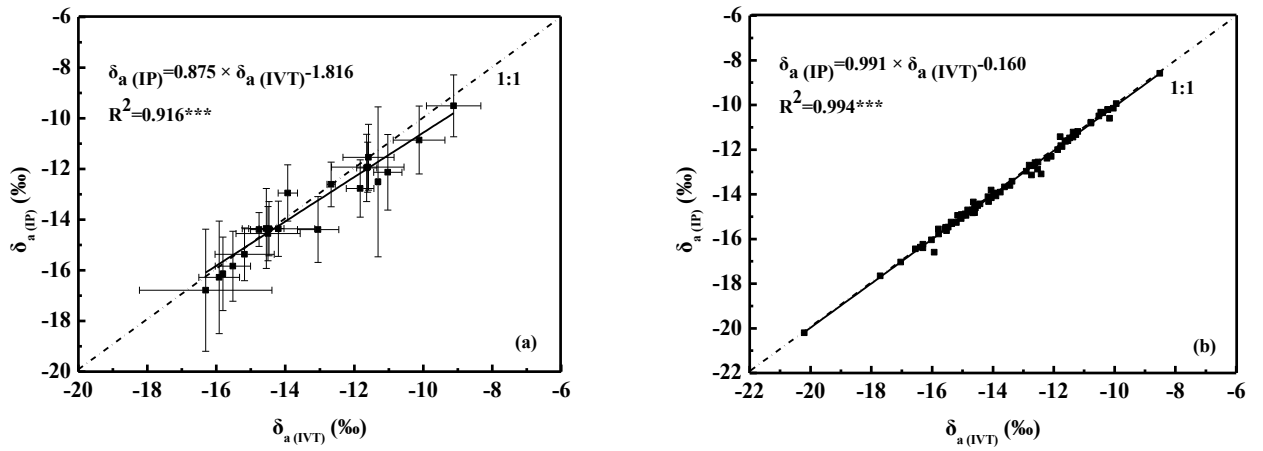


Fig. 4 Linear regression between the estimated isotope composition of ambient vapor using the intersection point method ($\delta_{a(\text{IP})}$) and the Intermediate Theorem method ($\delta_{a(\text{IVT})}$) on daily scale (a) and point to point scale (b), respectively.

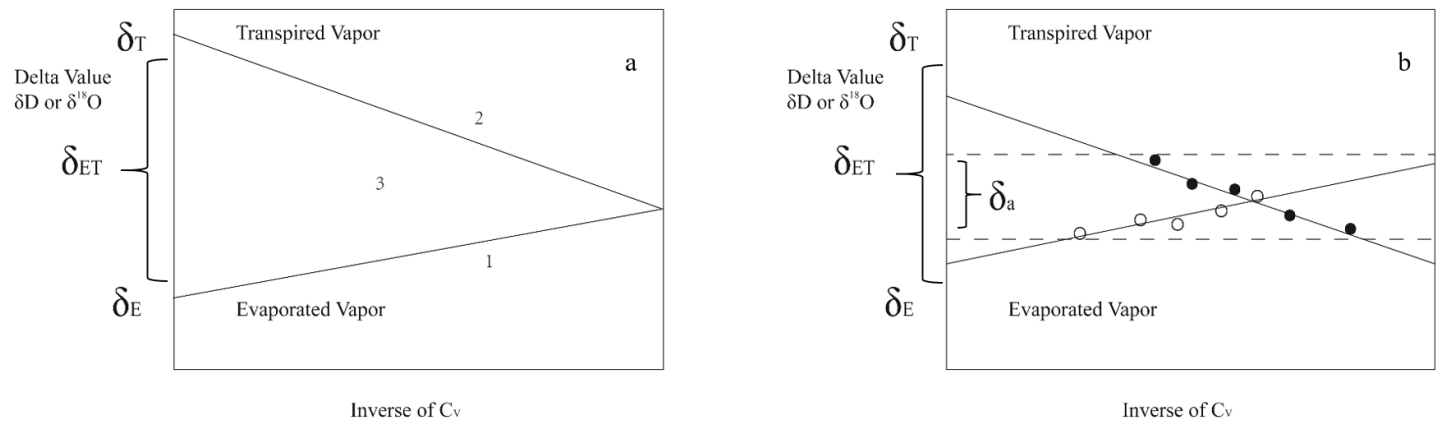


Fig. 5 Hypothetical graph of the idealized Keeling plots of the isotope composition of evaporation vapor (δ_E) (line 1), the isotope composition of transpiration vapor (δ_T) (line 2) and the isotope composition of evapotranspiration vapor (δ_{ET}) (area 3) (a), and hypothetical graph of idealized δ_E , δ_T lines and the interval of possible the isotope composition of ambient vapor (δ_a) in the Keeling plots (b).

Deleted: curve

Deleted: curve

Deleted: curve

Deleted: curve